Monitoring riverine traffic from space: The untapped potential of remote sensing for measuring human footprint on inland waterways

Magdalena Smigaj [a,b,*], Christopher R. Hackney [b], Phan Kieu Diem [c], Van Pham Dang Tri [d], Nguyen Thi Ngoc [e], Duong Du Bui [e], Stephen E. Darby [f], Julian Leyland [f]

[a] Laboratory of Geo-Information Science and Remote Sensing, Wageningen University & Research, Droevendaalsesteeg 3, 6708 PB Wageningen, the Netherlands
[b] School of Geography, Politics and Sociology, Newcastle University, Newcastle upon Tyne NE1 7RU, UK
[c] College of the Environment and Natural Resources, Can Tho University, 3/2 Street, Can Tho City, Viet Nam
[d] DRAGON-Mekong Institute, Can Tho University, 3/2 Street, Can Tho City, Viet Nam
[e] National Center for Water Resources Planning and Investigation (NAWAPI), Ministry of Natural Resources and Environment (MONRE), Hanoi, Viet Nam
[f] School of Geography and Environmental Science, University of Southampton, Southampton, UK

HIGHLIGHTS

- River traffic can be effectively monitored with satellite imagery and deep learning.
- In the Vietnamese Mekong Delta (VMD) we achieved boat detection accuracies of 84–85 %.
- We developed Human Waterway Footprint (HWF) products to map river traffic activity.
- HWF analysis showed human activity on VMD waterways increased by 25 % over 2018–2021.
- HWF contributes to assessment of environmental impacts of anthropogenic activities.

GRAPHICAL ABSTRACT
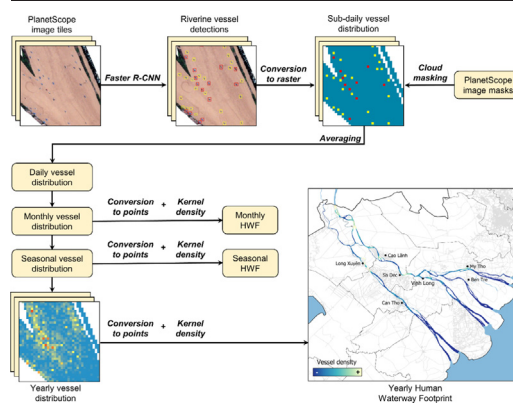
ARTICLE INFO

ABSTRACT

Mass urbanisation and intensive agricultural development across river deltas have driven ecosystem degradation, impacting deltaic socio-ecological systems and reducing their resilience to climate change. Assessments of the drivers of these changes have so far been focused on human activity on the subaerial delta plains. However, the fragile nature of deltaic ecosystems and the need for biodiversity conservation on a global scale require more accurate quantification of the footprint of anthropogenic activity across delta waterways. To address this need, we investigated the potential of deep learning and high spatiotemporal resolution satellite imagery to identify river vessels, using the Vietnamese Mekong Delta (VMD) as a focus area. We trained the Faster R-CNN Resnet101 model to detect two classes of objects: (i) vessels and (ii) clusters of vessels, and achieved high detection accuracies for both classes (f-score = 0.84–0.85). The model was subsequently applied to available PlanetScope imagery across 2018–2021; the resultant detections were used to generate monthly, seasonal and annual products mapping the riverine activity, termed here the Human Waterway Footprint (HWF), with which we showed how waterborne activity has increased in the VMD (from approx. 1650 active vessels in 2018 to 2070 in 2021 - a 25 % increase). Whilst HWF values correlated well with population density estimates (R^2 = 0.59–0.61, $p < 0.001$), many riverine activity hotspots were located away from population centres and varied spatially across the investigated period, highlighting that more detailed

* Corresponding author at: Laboratory of Geo-Information Science and Remote Sensing, Wageningen University & Research, Droevendaalsesteeg 3, 6708 PB Wageningen, the Netherlands.
E-mail address: magdalena.smigaj@wur.nl (M. Smigaj).

information is needed to fully evaluate the extent, and type, of human footprint on waterways. High spatiotemporal resolution satellite imagery in combination with deep learning methods offers great promise for such monitoring, which can subsequently enable local and regional assessment of environmental impacts of anthropogenic activities on delta ecosystems around the globe.

1. Introduction

Deltas are landscapes which, by their very nature, are defined by water. Globally, they are home to over 300 million people and provide some of the most fertile land for agriculture (Edmonds et al., 2020). Throughout history, many early civilisations (for example, the Ancient Egyptian civilization on the Nile, and the Harappan culture on the Indus) developed in deltaic regions due to the provision of productive agricultural land and good transport links for trade. In the past century, the world's deltas have seen major changes in their natural water and sediment regimes as a result of increasing human pressures both within delta regions and as a consequence of changes within their feeder basins upstream (Dunn et al., 2019). Mass urbanisation and intensive agricultural development across delta plains have driven a decline in biodiversity and ecosystem degradation, impacting deltaic socio-ecological systems and reducing their resilience to climate change (Tessler et al., 2015). Yet, assessments of the drivers of these changes have so far been focused on human activity on the subaerial delta plains rather than on the network of channels within deltas.

Analysis of the human footprint at global and regional scales (e.g. Sanderson et al. (2002), Venter et al. (2016)) often focuses purely on land, ignoring the distribution and intensity of waterway use completely. Where considered, the human impact on navigable waterways tends to be treated as being inversely weighted to the closest population centre (Venter et al., 2016). Although applicable at large scale, such approaches belie the importance these waterways have played throughout human history as conduits for transport, trade and regional connectivity. More importantly, they fail to account for the continuing importance of rivers in modern delta systems for food provision, transport and commerce, the provision of development materials (Bendixen et al., 2021), their role in driving delta-wide changes in salinity and flood risk (Vasilopoulos et al., 2021), and potential in reversing recent trends in freshwater biodiversity declines (Tickner et al., 2020). The fragile nature of deltaic ecosystems and the need for biodiversity conservation on a global scale require more accurate quantification of the footprint of anthropogenic activity across delta waterways.

The advent of high spatiotemporal resolution satellite imagery, developments in artificial intelligence, and increases in computational processing power have together now opened up the possibility of mapping riverine vessel activity over large spatial extents. Deep learning, a subfield of artificial intelligence, has seen a significant increase in popularity in recent years and is emerging as the leading tool for computer vision tasks, such as object detection and recognition, scene reconstruction, and video motion analysis. Its potential for monitoring pedestrian, vehicular, and water traffic with the use of surveillance cameras has been widely demonstrated (Chen et al., 2021; Chen et al., 2020; Zhou et al., 2018). Similarly, a range of studies have demonstrated that deep learning can also be successfully applied to very high resolution satellite imagery for detection of a range of objects, including motorised traffic (Froidevaux et al., 2020), infrastructure (Monna et al., 2021), and wildlife (Duporge et al., 2021; Guirado et al., 2019). Nevertheless, ship detection has so far focused heavily on the marine (Zhang et al., 2021; Nie et al., 2020) and lacustrine environments (Duan et al., 2019), with limited efforts, largely based on thresholding, within riverine and estuarine settings (Zhang et al., 2019; Gruel et al., 2022; Gruel and Latrubesse, 2021; Hackney et al., 2021).

This study, therefore, investigates whether riverine traffic activity can be effectively monitored at delta scale using deep learning approaches based on high spatiotemporal resolution satellite imagery, focusing on the Vietnamese Mekong Delta (VMD) as a case study. We applied this new workflow to develop products mapping this type of anthropogenic activity, termed here the Human Waterway Footprint (HWF), and subsequently addressed the following research questions: (i) how does the HWF spatially and temporally vary across the VMD throughout the 2018–2021 period, (ii) is activity on the VMD waterways closely related to the proximity to population centres?

2. Material and methods

2.1. Study site

The Vietnamese Mekong Delta (VMD) is home to approximately 17 million people, of whom 5.8 million live within 5 km of the main river network (General Statistics Office of Vietnam, 2021). There are two main waterways in the VMD, the Tien and Hau (Mekong and Bassac, respectively) rivers. The VMD is low-lying, with an average ground elevation of 0.7–1.2 m, with major population centres such as Can Tho (population ~ 1.2 million) and Vinh Long (population 0.2 million) located along the major waterways (Fig. 1). The livelihoods of the local population are reliant upon the productive agriculture and aquaculture supported by the delta and substantive supporting infrastructure. Beyond their role for food provision, transport and commerce, the waterways also have a high cultural value for the communities (Ehlert, 2012; Osborne, 2000). The composition of the waterway traffic is diverse, from small boats used for local navigation, through barges used for in-channel sand excavation or transport of goods within the VMD, to large trans-delta cargo vessels. Monitoring of any of this traffic is currently extremely limited.
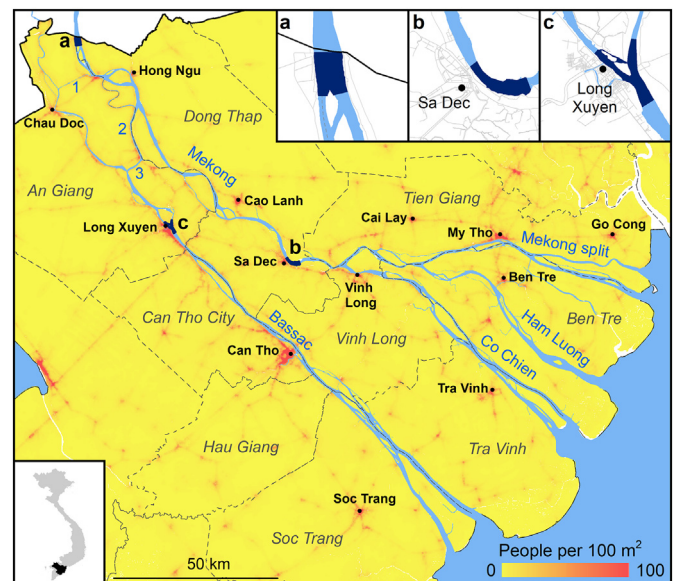

Fig. 1. The estimated population density in the Vietnamese Mekong Delta (VMD) based on WorldPop (2020) data. The boundaries of provinces and municipalities which contain main river channels are shown in grey, with major urban areas named. The main waterways are annotated in blue: Mekong, Bassac, 1 - Tan Chau - Chau Doc canal, 2 - Mekong-Vam Nao channel, 3 - Vam Nao, Mekong split, Ham Luong, Co Chien. Insets show sites where monthly temporal analysis of waterborne traffic was performed: near (a) the Vietnam-Cambodia border - 4.74 km², (b) Sa Dec - 4.36 km², (c) Long Xuyen - 4.00 km². Respective areas used for the analysis are shown in dark blue.

2.2. Remote sensing data

Satellite imagery from the PlanetScope constellation (Planet Team, 2017) that currently comprises approximately 130 "Dove" nano-satellites was used. This constellation is superior in terms of spatiotemporal resolution, offering an unprecedented combination of one-day revisit time and a ground sampling distance of approximately 3.7 m (nadir). As such, it has great potential for developing near-real time monitoring. We restricted the search to images that contained <10 % cloud cover, had a spatial resolution of ≤4 m, were acquired within the 1 January 2018–31 December 2021 period, and cumulatively covered at least 10 % of the study area on a given day. The obtained images were clipped to river extents (with a 100 m inland buffer) and sliced into 640 × 640 pixel image tiles to make them compatible for deep learning.

2.3. Deep learning workflow for the detection of river vessels

The analysis was restricted to large river vessels (defined here as >20 m in length), which we judged to be the minimum detectable size. Two classes of objects were used: (i) vessels and (ii) clusters of vessels, where multiple vessels were moored together, preventing effective separation at this spatial resolution. To ensure that a representative and diverse image sample was used for training purposes (to capture variability in both vessel type and background river turbidity conditions), we utilised images captured in different seasons – one for each month of the year 2020 (Table 1); the exact days were randomly chosen from the pool of available imagery. The selected image tiles were then randomly split into training (80 %) and validation sets (20 %) to allow selection of the best model for vessel detection. The selected image tiles were annotated by defining bounding boxes around each vessel or a cluster of vessels with the LabelImg tool (Tzutalin, 2015). In total, 8274 instances of individual vessels and 2198 instances of clusters of vessels were used for training and validation purposes (Table 1).

The Faster R-CNN Resnet101 model (Ren et al., 2015; He et al., 2016) was selected as most appropriate in terms of the trade-off between performance and inference time. It was trained using Tensorflow, implemented through Google Colaboratory, for 60,000 iterations with a learning rate of 0.01, batch size of 2 and a non-maximum suppression intersection oven union (IoU) threshold of 0.4. Precision-recall (PR) curves and mean Average Precision metrics (mAP and mAP50) were used to assess its performance – based on these a confidence threshold of 0.3, which kept the precision and recall rates balanced, was selected for further application. For the calculation of mAP ten IoU levels were used, starting from 0.50 to 0.95 (with a step size of 0.05), whilst for mAP50 a single IoU threshold of 0.50 was used. Comparisons against other tested models, input tensor sizes and learning rates, as evaluated on the validation dataset, are available in the Supplementary Material. The post training performance of the model was assessed using imagery from two additional randomly chosen days, which served as an independent test dataset with a total of 2649 instances of individual vessels and 633 instances of clusters of vessels (Table 1). For each class, precision, recall and f1-score were calculated for evaluation purposes. A match was recognised only when a model detection's centroid intersected its corresponding reference bounding box annotation. The trained Faster R-CNN Resnet101 model was subsequently applied to all acquired PlanetScope imagery.

2.4. Generation of Human Waterway Footprint (HWF) products

Centroids of the model detections were used to derive monthly and yearly Human Waterway Footprint (HWF) products across the VMD following the workflow presented in Fig. 2. First, detections from each satellite acquisition were converted into raster layers covering only river extents (50 m pixel size). During the conversion "vessel" detections were given a value of 1 and "cluster" detections were given a value of 2.6, which was the average number of vessels in a cluster in the test datasets (based on visual interpretation). A cloud mask provided by Planet was subsequently applied to each raster set. Next, these sub-daily raster layers were averaged to derive daily boat distributions and account for overlap between acquisitions from different satellites. Similarly, monthly/seasonal/yearly distributions were derived by averaging the corresponding daily/monthly/seasonal raster layers. Final HWF products were generated by first converting these raster layers into points that were then used as inputs for a weighted kernel density estimator from the Spatstat R package version 2.2–0 (Baddeley and Turner, 2005) with quartic kernel type, bandwidth of 1 km, and raster averages as input weights. Our HWF products, therefore, provide an estimation of the river traffic intensity per km^2 on an average day in a given month/season/year. For the generation of seasonal HWF products we differentiated between the dry season (November–April) and the wet season (May–October). The seasonal split was implemented to ensure the derived interannual variation is not affected by lower image availability in the wet season when cloud cover is more prevalent.

To explore the relationship between our HWF products and delta-top human activity we investigated how well the annual HWF products correspond with population density estimates based on available WorldPop (2018, 2019 and 2020) data. For this purpose, the selected WorldPop layers were first resampled to HWF's spatial resolution. Approximate population density values for the water pixels were then obtained through a circular focal filter (average) with a radius of 4 km. A 4 km radius was chosen to reflect the distance over which an increased traffic activity due to the presence of a population centre would be expected. Pairwise pixel observations of this density layer and annual HWF products were then extracted for each year and Pearson's correlation coefficient computed following log scale data normalisation. We also tested 1, 2, 3 and 5 km radius values for the population density estimates – these, with the exception of the 1 km radius, produced similar outcomes, which are available in the Supplementary Material.

Table 1

Table 1. List of satellite image acquisition days used for the training and validation (Train/Val) and test datasets (Test), alongside respective number of class instances.

| Acquisition day	No. of satellites	Satellite IDs	No. of tiles	Dataset	'Vessel' instances	'Cluster' instances
10.01.2020	7	0e3a, 0f25, 0f28, 0f33, 1004, 1006, 106f	716	Train/Val	1172	265
03.02.2020	5	0f28, 0f2a, 1004, 1006, 1040	360	Train/Val	273	56
24.02.2020	7	0e19, 0f49, 100d, 105a, 106d, 1008, 1014	762	Test	2040	448
28.03.2020	3	103e, 1043, 106d	271	Train/Val	664	177
30.04.2020	7	0f32, 0f36, 1011, 1012, 1027, 1034, 2277	721	Train/Val	1188	231
16.05.2020	1	1049	150	Train/Val	497	153
06.06.2020	3	0f2b, 1008, 1014	131	Train/Val	449	135
25.07.2020	1	104b	143	Train/Val	143	48
21.08.2020	2	1003, 1049	186	Train/Val	555	105
08.09.2020	3	0f2b, 1053, 2304	223	Test	609	187
16.09.2020	4	0e3a, 0f32, 0f46, 103b	340	Train/Val	857	263
24.10.2020	3	1040, 1061, 2235	208	Train/Val	454	150
13.11.2020	3	1035, 1053, 105e	152	Train/Val	336	87
03.12.2020	7	0f15, 0f3c, 1014, 103b, 106d, 2259, 2426	805	Train/Val	1686	528
Total	46		4183	Train/Val	8274	2198
Total	10		985	Test	2649	635
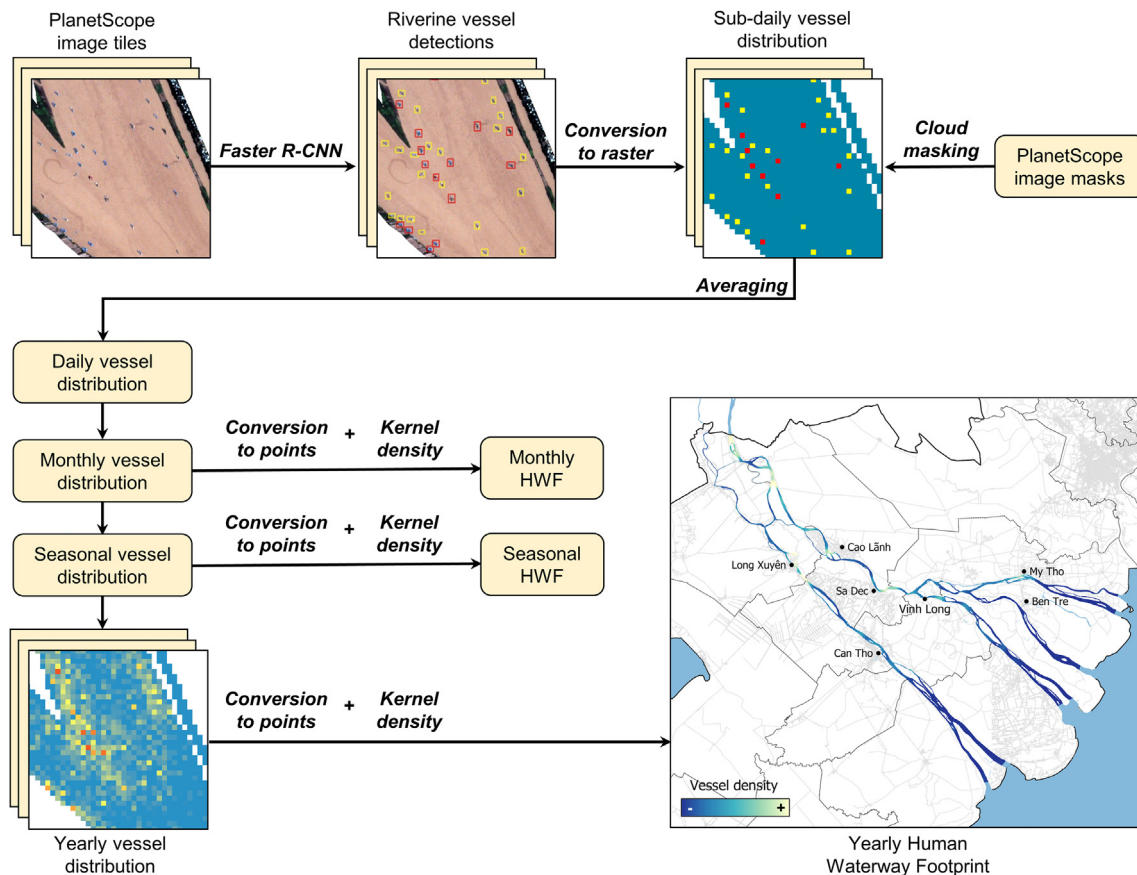
Fig. 2. The workflow for generation of yearly and monthly Human Waterway Footprint products. Individual vessels are marked in yellow, whilst clusters of vessels in red.

2.5. Spatiotemporal variations in HWF across the delta

The annual HWF products were used to analyse the variation in traffic activity levels across the investigated years. For each of the nine provinces (see Fig. 1 for reference), we calculated the daily number of vessels in a given year by extracting the average value from the corresponding annual HWF and multiplying it by the river area of a given province. This provided an estimate of the total number of vessels present within each province/municipality on an average day in a given year. We performed analogous calculations of the total number of vessels for each of the eight main waterways in the VMD (see Fig. 1 for reference).

Additionally, we used the monthly HWF products to explore the month-to-month variation in the number of vessels for three distinct river sections located near: (a) the Vietnam-Cambodia border on the Mekong channel, (b) Sa Dec on the Mekong channel, (c) Long Xuyen on the Bassac channel. These are shown in Fig. 1 and cover areas of 4.74, 4.36 and 4.00 km^2 respectively. We selected sites (b) and (c) as examples of waterborne activity in proximity to population centres, and site (a) as an example of activity focusing on in-channel sand extraction. For each month, the average number of PlanetScope images used for generation of the monthly HWF layers across the period 2018–2021 was also counted to provide a qualitative confidence measure for the derived traffic intensity.

3. Results

3.1. Riverine vessel detection performance and generation of HWF products

The applied workflow allowed successful identification of riverine traffic with the trained model achieving mAP of 0.52 and mAP50 of 0.90. Though, detections of vessel clusters had higher uncertainty levels as indicated by the precision-recall curves provided in the Supplementary material. A sample

scene with resultant detections is shown in Fig. 3, whereas further model evaluation metrics derived from the independent dataset are available in Table 2. On both tested days, the model achieved high detection accuracy for both individual vessels (f-score = 0.84–0.85) and clusters of vessels (f-score = 0.84–0.85), with errors of omission and commission well balanced; detailed confusion matrices are provided in the Supplementary Material. Vessels which remained undetected were often moored at the riverbank, making them difficult targets. Conversely, river huts were occasionally mistaken for clusters of vessels due to their similar overall appearance. Confusion between the two classes also occurred but very sporadically, accounting for approximately 3 % of all detections.

The developed model was subsequently applied to the available PlanetScope imagery meeting the search criteria; in total, we obtained detections from varying spatial extents from 114 days in 2018, 96 days in 2019, 145 days in 2020, and 129 days in 2021. For an average pixel within the delta, this translated to 38 separate days of information on waterborne activity that contributed towards the generation of our annual HWF products. The number of days was dictated by image availability in a given year, which was influenced by the number of Dove satellites in orbit at the time, and cloud conditions. In particular, the monsoon season proved problematic for ensuring adequate data coverage. In the case of monthly HWF products, where no information on vessel occurrence was available for an area in a given month, we retained null values. Despite these limitations, satisfactory coverage for derivation of annual HWF products was achieved, all of which were calculated from at least six monthly HWF layers. The largest data gaps occurred in 2018 when 27 % of the VMD area was covered by less than nine monthly composites. In contrast, in 2019–2021 nine or more monthly composite values were available for over 95 % of the VMD. A visual summary and additional information on the coverage of the monthly and annual HWF products across 2018–2021 are provided in the Supplementary Material.
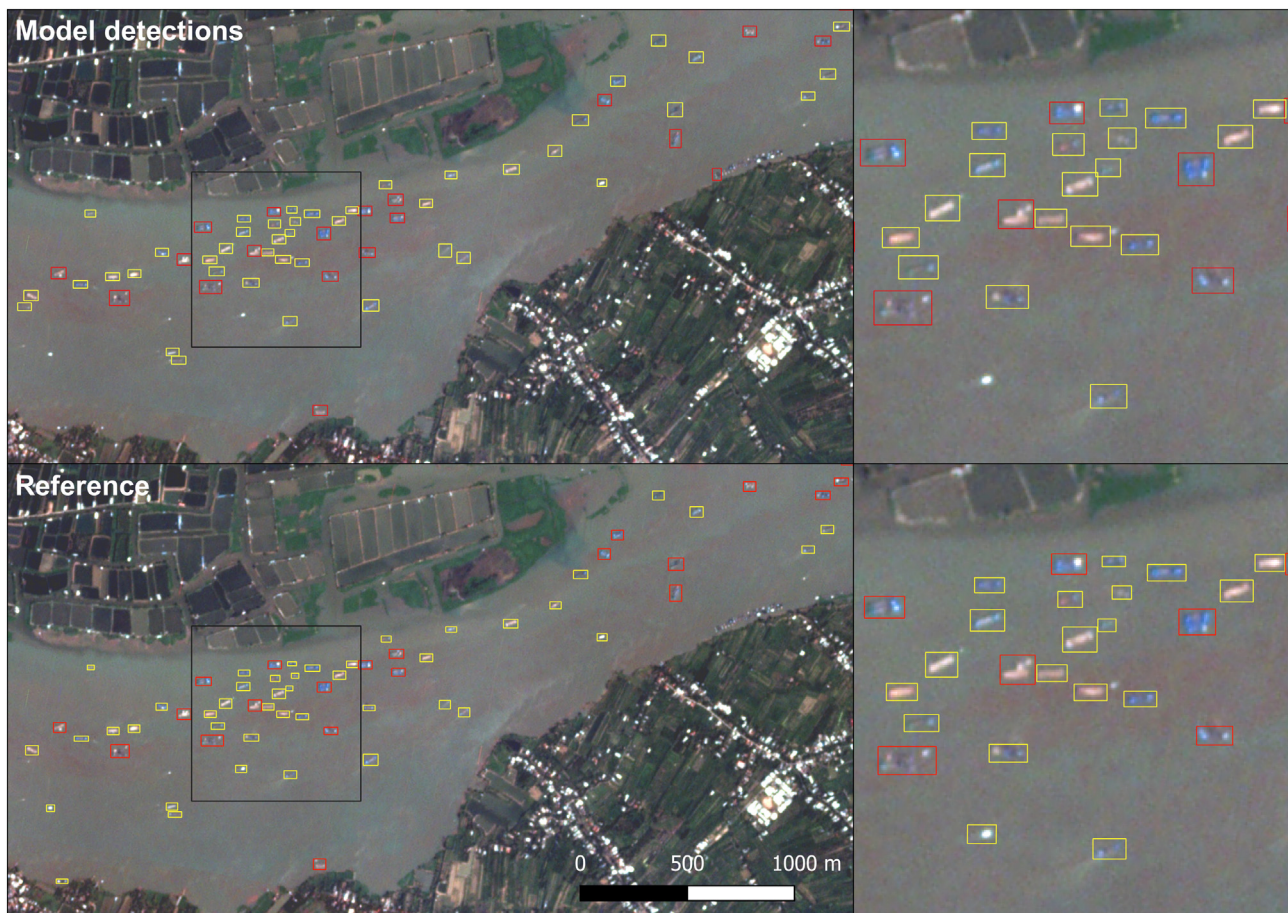
Fig. 3. Sample results of the riverine vessel detection workflow (top) and the reference (bottom) near Sa Dec – 10°17′10″N 105°47′40″E. Individual vessels are shown in yellow, whilst clusters of vessels are shown in red. Background: PlanetScope imagery from 24.02.2020.

3.2. Anthropogenic activity across the VMD waterways

A sample annual HWF product, portraying vessel density across the VMD in 2021, is shown in Fig. 4.a. Areas experiencing heightened pressure from waterborne traffic, located in the middle and upper reaches of the delta in particular, are clearly evident. Some of these are near the major population centres. At the delta scale, we observed a clear relationship between the HWF products and population density estimates (Fig. 4.c). The increasing trend of activity levels was consistent for all of the investigated years (similar trendline slopes) with R^2 values in the range of 0.59–0.61. Nevertheless, many of the 2021 activity hotspots were located away from densely populated areas. Over the course of the 4 years investigated here (2018–2021) major shifts in hotspot distribution in the Mekong River occurred (Fig. 4.b), demonstrating the dynamic nature of the waterborne anthropogenic activity that cannot be fully captured with population density estimates. Conversely, in the Bassac river a general increase in activity

can be seen (increase from the average of 1.35 vessels per km^2 in 2018 to 1.91 vessels per km^2 in 2021 across the full length of the river).

Both province-level and channel-level estimates of the total number of vessels present per day exhibited varied multitemporal patterns (Fig. 5). Most provinces exhibited similar activity levels over the course of the four investigated years. Among the exceptions were An Giang that experienced a steady rise and Can Tho municipality where a step increase occurred in 2019. These changes were reflected in the Bassac, the Mekong and the Mekong - Vam Nao channel estimates. The sharp increase in Can Tho municipality corresponds well with local reports on the acceleration of illegal sand and clay mining (Vnexpress, 2020a). Illegal mining activities have also become pervasive in An Giang because of the sand quality and availability in this province (MONRE, 2015, Le Manh Hung, 2013). Dong Thap similarly observed a substantial increase in the number of vessels until 2021. This peak coincides with relaxed regulation of riverine traffic observed during COVID-19 lockdown restrictions in 2020 (Vnexpress,

Table 2
Accuracy measures for the developed vessel detection approach. The "combined" class is given to show the overall performance, i.e. a successful detection of either a vessel or a cluster.

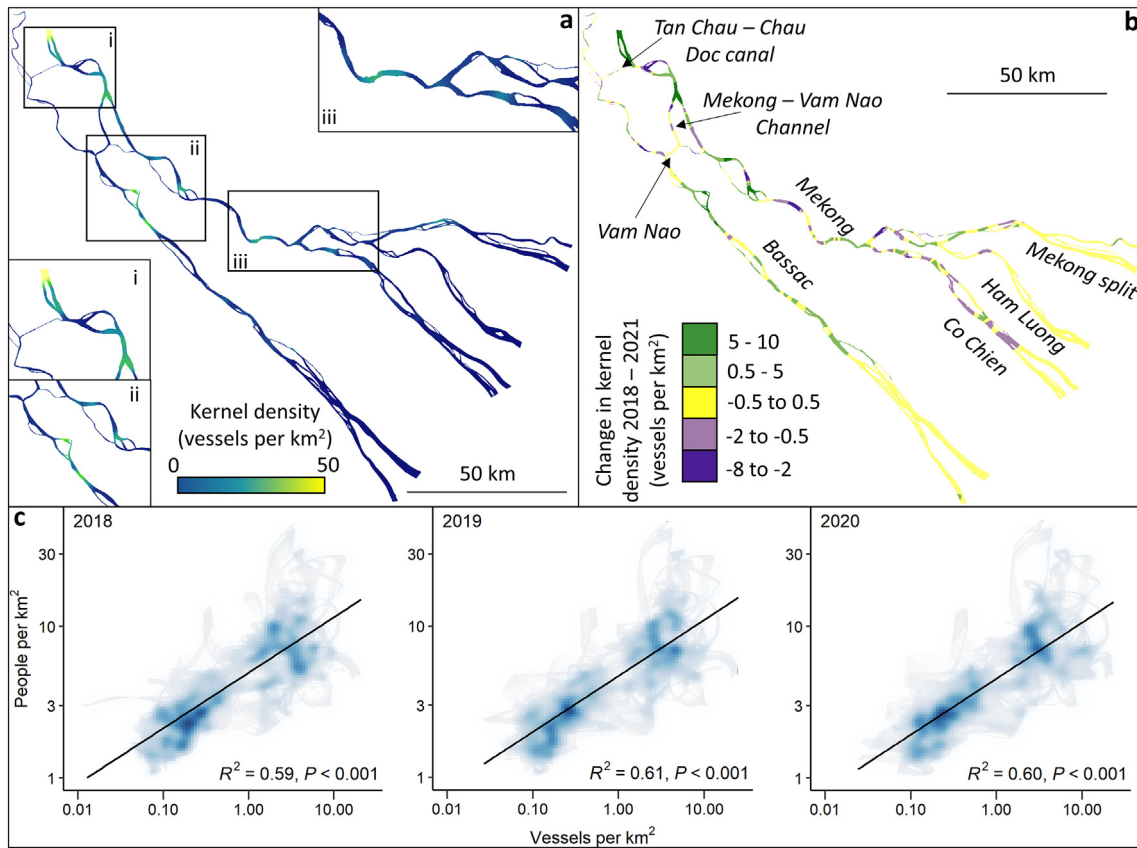| Date	Class	No. of features	No. of detections	True positive	False negative	False positive	Precision	Recall	F score
24.02.2020	Vessel	2040	1963	1672	368	291	0.85	0.82	0.84
	Cluster	448	394	357	91	37	0.91	0.80	0.85
	Combined	2488	2357	2093	395	264	0.89	0.84	0.86
08.09.2020	Vessel	609	606	518	91	88	0.85	0.85	0.85
	Cluster	187	176	152	35	24	0.86	0.81	0.84
	Combined	796	782	701	95	81	0.90	0.88	0.89

Fig. 4. Annual HWF for 2021 (a); boxes along the main river channels relate to zoomed in insets identified by numerals within each box. (b) Difference in kernel density between annual HWF for 2018 and 2021 with the main channels of the VMD labelled. (c) Colour shaded scatterplots between annual HWF and population density values extrapolated from WorldPop (2018, 2019, 2020) data.
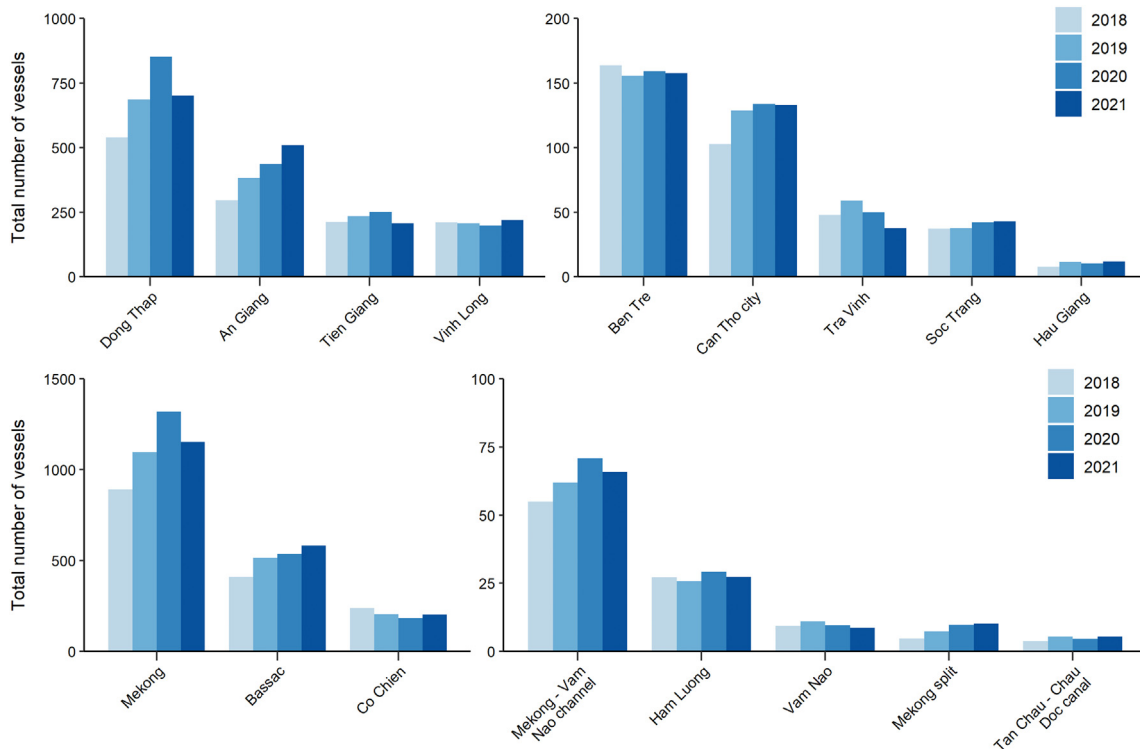

Fig. 5. Number of vessels on an average day for the period 2018–2021 for each province/municipality (*top*) and river channel (*bottom*) within the VMD.

2020b); in the following year with the return to normalcy the activity levels were on par with those in 2019. A similar pattern was observed at the delta scale, with an increase from approx. 1650 vessels in 2018 across the VMD through 1950 in 2019 reaching 2180 in 2020, followed by a drop to 2070 vessels in 2021.

3.3. Local monitoring of the riverine traffic intensity

Monthly HWF products generated here can provide useful insights into riverine traffic patterns at the provincial level. Fig. 6 portrays the temporal variation in waterborne activity at three distinct river sections, revealing substantial differences in traffic volume and in inter-annual trends of activity. Near the Vietnam-Cambodia border on the Mekong channel we observed a high concentration of vessels that according to the trendline (see dotted line on Fig. 6) consistently exceeded 60 vessels within an area of 4.74 km^2 (>12.7 vessels per km^2). Throughout the investigated period a significant increase in vessel numbers occurred, which accelerated from the beginning of 2020. By the end of 2021 the number of vessels in the area doubled compared to 2018 levels, reaching 158 vessels (or 33.5 vessels per km^2, based on the trendline estimates, compared to 15.7 vessels per km^2). These changes can be attributed to the increase in the in-channel sand mining activity in this region, which has been reported in recent years (Gruel et al., 2022; Vnexpress, 2020a).

Conversely, near Sa Dec, vessel numbers have been diminishing since 2020 when we observed a peak of waterborne activity - approx. 56 vessels within an area of 4.36 km^2 based on the trendline values (12.9 vessels per km^2). This peak can similarly be attributed to in-channel sand mining, which could not be effectively regulated during the introduction of COVID-19 restrictions (Vnexpress, 2020b). By the end of 2021 the traffic intensity levels substantially decreased (5.6 vessels per km^2), reflecting

those from the beginning of 2018 (4.7 vessels per km^2). The final site near Long Xuyen experienced consistently low traffic until 2020 (4.3 vessels per km^2 based on the trendline estimates). A steep increase followed at the end of 2020 and throughout 2021 when the number of vessels within this river section tripled compared to 2018 levels, reaching 51 vessels (12.8 vessels per km^2).

For each of these three sites, we also included the average number of PlanetScope images used for the generation of monthly HWF products to serve as a qualitative measure for the traffic estimates (Fig. 6). These highlight lower data availability during the monsoon season months. Nevertheless, the extracted traffic estimates appeared largely insensitive to the changing number of input images - there was no significant correlation between the number of used images and the resultant number of detected vessels.

4. Discussion

This study is the first to identify and map riverine vessels at the delta scale, in an attempt to characterise the human footprint on delta waterways. Our study demonstrates that deep learning approaches, in combination with high spatiotemporal resolution satellite imagery, have high potential for performing such tasks across large spatial extents. Although the spatial resolution of satellite imagery employed here (PlanetScope, ~3.7 m at nadir) prevented effective separation of individual vessels when they were moored together, we were still able to train the Faster R-CNN model to identify and differentiate individual vessels and clusters of vessels, achieving high f-scores of 0.84–0.85. Missed detections were generally located at the riverbank, which made them difficult targets due to visual overlap. Detection of small objects in imagery (relative to pixel size) is a well-known challenge in the computer vision domain and an ongoing area of research. Whilst many improvements have been made over the years, a large disparity in detection performance between small and medium-to-large objects still exists (Nguyen et al., 2020). Computationally intensive two-stage approaches, such as Faster R-CNN, are therefore still preferable for small objects owing to their superior accuracy (Nguyen et al., 2020). Employment of ultra-high spatial resolution satellite imagery (e.g. Worldview) would alleviate this issue by increasing the information content; such imagery was previously successfully used as input for deep learning for detection of a wide range of targets of varying sizes (Duporge et al., 2021; Froidevaux et al., 2020; Guirado et al., 2019; Zhang et al., 2019). However, very high costs associated with such imagery would currently render this solution infeasible for continuous monitoring across the extensive spatial areas of large deltas.

High spatiotemporal resolution satellite imagery in combination with deep learning methods offer great promise for monitoring waterborne anthropogenic activity over large spatial extents. The approach employed in this study for riverine vessel detection could be extended to other waterways, following optimisation for local characteristics with supplementary training data. Here, for training purposes we utilised imagery acquired in different seasons to ensure the variability in both vessel type and sediment conditions was captured. Such monitoring approaches can prove invaluable for capturing shifts in activity and enable assessment of environmental impacts of human activities on freshwater ecosystems around the globe. The main limitation is the use of optical satellite imagery, and specifically its susceptibility to cloud cover that can significantly limit data availability, especially during the cloudy monsoon season. Whilst PlanetScope's high temporal resolution and overlapping of satellite footprints maximises the chances of obtaining suitable imagery, data gaps were still noticeable, especially in 2018 when only 73 % of the VMD area was covered by 9 or more monthly composites (versus 95–99.96 % in 2019–2021). Approaches utilising Synthetic Aperture Radar (SAR) imagery, which are not affected by cloud cover, could potentially supplement the analysis by filling these temporal data gaps. SAR has long been utilised for marine surveillance with a range of traditional feature-based (Eldhuset, 1996; Iervolino and Guida, 2017; Yang et al., 2019) and deep learning (Jin et al., 2020; Zhang et al., 2021; Zhang et al., 2020) approaches developed over the years.
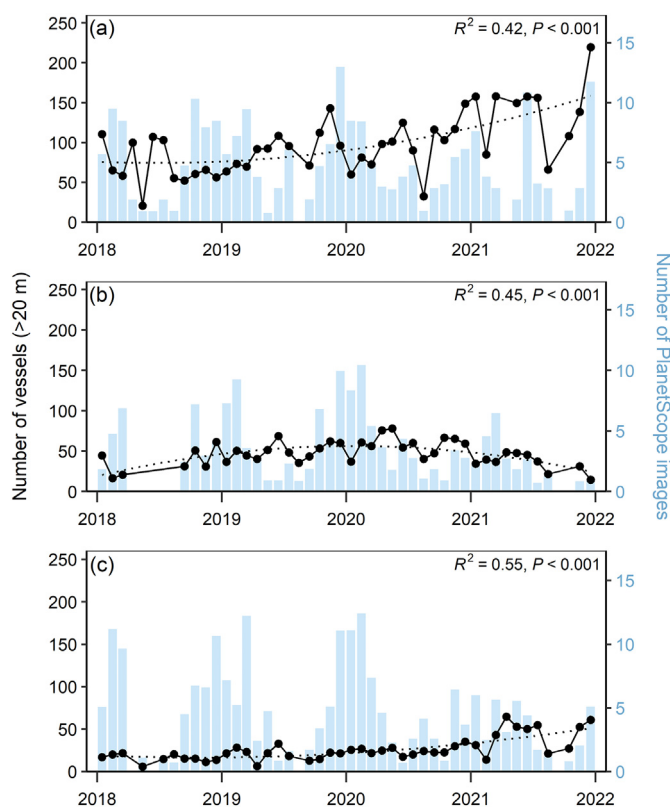

Fig. 6. Daily number of vessels >20 m in length during the period 2018 to 2021 alongside the average number of PlanetScope images used for the generation of monthly HWF within the sample area near (a) the Vietnam-Cambodia border, (b) Sa Dec, and (c) Long Xuyen (see Fig. 1 for reference). Dotted lines represent second order polynomial trend lines.

However, only limited attention has been given to riverine settings, with a focus on the detection of large vessel clusters (≥70 m in length) with Sentinel-1 imagery (Gruel et al., 2022; Gruel and Latrubesse, 2021). Similarly as in the optical domain, a trade-off between spatial resolution and imagery costs is required, significantly limiting options for implementation of continuous monitoring. The approaches utilising Sentinel-1 imagery potentially omit a significant proportion of vessels operating on the river, thus underestimating levels of activity; whilst Gruel et al. (2022) estimated there were on average approx. 350 active vessels across the VMD in 2020, our workflow identified the presence of approx. 2180 vessels. Nonetheless, fusion of the two modalities would be worthy of further exploration to improve data continuity.

Typically, measures of human impact on landscapes have focussed on the terrestrial environments, with land use and land cover maps used to assess human activity and changes in the terrestrial biospheres (Fritz et al., 2017; Sanderson et al., 2002). These products are invaluable for assessing human alterations to ecosystem service provision (Daily and Ruckelshaus, 2022), protecting and managing vital landscapes and in developing sustainable management plans. However, they ignore the importance of rivers and other waterways as a key provider of ecosystem services and as a locus for anthropogenic impact. Anthropogenic impacts on, and in, global waterways are increasingly being recognised (Hackney et al., 2020; Meijer et al., 2021; Wilkinson et al., 2022), with the reported rapid decline of freshwater biodiversity among the most concerning (Albert et al., 2021). Our ability to capture spatiotemporal trends in waterway use is vital for understanding the role that waterway use plays in driving and propagating changes in the freshwater environment. The generated HWF layers gave valuable insights into the changing human pressure levels across the VMD. At the delta scale we observed that waterborne activity increased by 25 % from 2018 to 2021 from approx. 1650 active vessels in 2018 to approx. 2070 in 2021, with most substantial increases in two upstream provinces: An Giang (72 % from approx. 297 to 510 vessels) and Dong Thap (30 % from approx. 539 to 701 vessels). The HWF activity hotspots in these provinces were located away from densely populated areas and could be related to known in-channel sand mining locations where river barges with excavators and transport vessels awaiting sand load are located in close proximity, forming large congregations. Similar increases were also recorded within the Can Tho city municipality (29 % from approx. 103 to 133 vessels) and Hau Giang (54 % from approx. 8 to 12 vessels). In contrast, in some downstream provinces a slight decrease in riverine traffic occurred, namely in Tra Vinh (−21 % from approx. 48 to 38 vessels), Ben Tre (−4 % from approx. 164 to 158) and Tien Giang (−2 % from approx. 212 to 207 vessels). Such shifts in waterway use that are not directly related to population growth and/or movement cannot be fully captured with terrestrial products. However, it should be noted that we did observe a clear relationship between the generated HWF products and population density estimates at the delta scale (R^2 values in the range of 0.59–0.61, $p < 0.001$).

A greater understanding of waterway use is essential for evaluation of environmental impacts of anthropogenic activities and development of appropriate remediation measures. For example, inland waterway traffic was shown to affect species richness and abundance in riverine ecosystems due to noise pollution (Slabbekoorn et al., 2010; Wang et al., 2020) and transfer of hydraulic forces into the water column, i.e. vessel-induced waves, currents and drawdowns (Zajicek and Wolter, 2019). With HWF, specific areas undergoing high pressure and/or that are key for conservation efforts can be targeted, e.g. by establishing protected areas. Subsequently, the effectiveness of introduced measures can be assessed through monitoring of changes to the anthropogenic activity levels. Here, the HWF is based solely on identified vessels >20 m, which is an important first step towards the partitioning out of the HWF by water use or activity type. A HWF that is able to identify types of activity (e.g. transportation (ferry), shipping, fishing, sand mining) could permit impact assessment of different activities on the freshwater environment. Further integration with terrestrial datasets, such as land use/land cover maps, with which information on e.g. agricultural run-off or industrial/domestic pollution can be derived, can give the full picture of the extent to which inland waterways are being affected by human activities. This can open up the opportunity for more synergistic, targeted and sustainable management plans that can achieve a better balance between nature, agriculture, resource abstraction and urban development.

5. Conclusions

Our study is the first to identify river vessels at the delta scale to characterise the human footprint on these vital waterways. We aimed to tackle the general lack of products addressing anthropogenic impacts on such waterways and the extremely limited monitoring of riverine traffic in the Vietnamese Mekong Delta (VMD) in particular. For this purpose, we employed Faster R-CNN Resnet101 model and PlanetScope imagery to detect two classes of riverine objects: (i) individual vessels and (ii) clusters of vessels, and achieved high detection accuracies (f-score = 0.84–0.85). We subsequently developed monthly, seasonal and annual Human Waterway Footprint (HWF) products from vessel detections obtained across the 2018–2021 period. These products provide an estimation of the average number of vessels per km^2 per day over a given month/year and give an insight into the spatiotemporal variability of vessel numbers across the VMD.

The developed annual HWF gave insights into the spatiotemporal variability of riverine anthropogenic activity, highlighting areas experiencing continuous heightened pressure from waterborne traffic. At the delta scale, we observed a clear relationship between the HWF products and population density estimates. Nevertheless, many of the activity hotspots were located away from densely populated areas, driven by resource extraction and transportation of goods. We showed how monthly HWF products can reveal substantial differences in traffic volume and in inter-annual trends of riverine activity at local level with two-fold (from 15.7 to 33.5 vessels per km^2) and three-fold (from 4.3 to 12.8 vessels per km^2) increases over the 2018–2021 period near the Cambodia-Vietnam border and Long Xuyen, respectively. At the delta scale we observed the waterborne activity increase by 25 % over 2018–2021.

Deep learning methods in combination with high spatiotemporal resolution satellite imagery offer great promise for monitoring waterborne anthropogenic activity over large spatial extents. Resultant products, such as HWF developed here, can prove invaluable for capturing shifts in riverine traffic, enabling assessment of environmental impacts of human activities on freshwater ecosystems around the globe and subsequent development of river management plans that can achieve a better balance between nature, agriculture, resource abstraction and urban development.

CRediT authorship contribution statement

Magdalena Smigaj: Data curation, Methodology, Formal analysis, Investigation, Validation, Visualization, Writing – original draft, Writing – review & editing. **Christopher R. Hackney:** Investigation, Visualization, Writing – original draft, Writing – review & editing. **Phan Kieu Diem:** Investigation, Writing – review & editing. **Van Pham Dang Tri:** Investigation, Writing – review & editing. **Nguyen Thi Ngoc:** Investigation, Writing – review & editing. **Duong Du Bui:** Investigation, Writing – review & editing. **Stephen E. Darby:** Writing – review & editing. **Julian Leyland:** Funding acquisition, Project administration.

Data availability

The generated monthly, seasonal and yearly HWF products will be made available for download through the Delta Portal (http://www.delta-portal.net/). Data from intermediate stages are available from the corresponding author upon reasonable request.

Declaration of competing interest

The authors declare they have no conflict of interests.

Acknowledgements

Appendix A. Supplementary data

Supplementary data to this article can be found online at https://doi.org/10.1016/j.scitotenv.2022.160363.

References

Albert, J.S., Destouni, G., Duke-Sylvester, S.M., Magurran, A.E., Oberdorff, T., Reis, R.E., Winemiller, K.O., Ripple, W.J., 2021. Scientists' warning to humanity on the freshwater biodiversity crisis. Ambio 50, 85–94.

Baddeley, A., Turner, R., 2005. spatstat: an R package for analyzing spatial point patterns. J. Stat. Softw. 12, 1–42.

Bendixen, M., Iversen, L.L., Best, J., Franks, D.M., Hackney, C.R., Latrubesse, E.M., Tusting, L.S., 2021. Sand, gravel, and UN sustainable development goals: conflicts, synergies, and pathways forward. One Earth 4, 1095–1111.

Chen, X., Qi, L., Yang, Y., Luo, Q., Postolache, O., Tang, J., Wu, H., 2020. Video-based detection infrastructure enhancement for automated ship recognition and behavior analysis. J. Adv. Transp. 2020, 7194342.

Chen, L., Grimstead, I., Bell, D., Karanka, J., Dimond, L., James, P., Smith, L., Edwardes, A., 2021. Estimating vehicle and pedestrian activity from town and city traffic cameras. Sensors 21, 4564.

Daily, G.C., Ruckelshaus, M., 2022. 25 years of valuing ecosystems in decision-making. Nature 606, 465–466.

Duan, H., Cao, Z., Shen, M., Liu, D., Xiao, Q., 2019. Detection of illicit sand mining and the associated environmental effects in China's fourth largest freshwater lake using daytime and nighttime satellite images. Sci. Total Environ. 647, 606–618.

Dunn, F.E., Darby, S.E., Nicholls, R.J., Cohen, S., Zarfl, C., Fekete, B.M., 2019. Projections of declining fluvial sediment delivery to major deltas worldwide in response to climate change and anthropogenic stress. Environ. Res. Lett. 14, 084034.

Duporge, I., Isupova, O., Reece, S., Macdonald, D.W., Wang, T., 2021. Using very-high-resolution satellite imagery and deep learning to detect and count African elephants in heterogeneous landscapes. Remote Sens. Ecol. Conserv. 7, 369–381.

Edmonds, D.A., Caldwell, R.L., Brondizio, E.S., Siani, S.M.O., 2020. Coastal flooding will disproportionately impact people on river deltas. Nat. Commun. 11, 4741.

Ehlert, J., 2012. Beautiful Floods: Environmental Knowledge And Agrarian Change in the Mekong Delta, Vietnam. LIT Verlag Münster.

Eldhuset, K., 1996. An automatic ship and ship wake detection system for spaceborne SAR images in coastal regions. IEEE Trans. Geosci. Remote Sens. 34, 1010–1019.

Fritz, S., See, L., Perger, C., McCallum, I., Schill, C., Schepaschenko, D., Duerauer, M., Karner, M., Dresel, C., Laso-Bayas, J.-C., Lesiv, M., Moorthy, I., Salk, C.F., Danylo, O., Sturn, T., Albrecht, F., You, L., Kraxner, F., Obersteiner, M., 2017. A global dataset of crowdsourced land cover and land use reference data. Sci. Data 4, 170075.

Froidevaux, A., Julier, A., Lifschitz, A., Pham, M.T., Dambreville, R., Lefèvre, S., Lassalle, P., Huynh, T.L., 2020. Vehicle detection and counting from VHR satellite images: efforts and open issues. IGARSS 2020 - 2020 IEEE International Geoscience And Remote Sensing Symposium, 26 Sept.-2 Oct. 2020, pp. 256–259.

General Statistics Office of Vietnam, 2021. Population And Housing Survey [Online]. General Statistics Office of Vietnam, Hanoi Available: https://www.gso.gov.vn/px-web-2/?pxid=V0201&theme=D%C3%A2n%20s%E1%BB%91%20v%C3%A0%20lao%20%C4%91%E1%BB%99ng [Accessed 01/06/2022].

Gruel, C.R., Latrubesse, E.M., 2021. A monitoring system of sand mining in large rivers and its application to the Ayeyarwady (Irrawaddy) river, Myanmar. Water 13, 2331.

Gruel, C.-R., Park, E., Switzer, A.D., Kumar, S., Loc Ho, H., Kantoush, S., van Binh, D., Feng, L., 2022. New systematically measured sand mining budget for the Mekong Delta reveals rising trends and significant volume underestimations. Int. J. Appl. Earth Obs. Geoinf. 108, 102736.

Guirado, E., Tabik, S., Rivas, M.L., Alcaraz-Segura, D., Herrera, F., 2019. Whale counting in satellite and aerial images with deep learning. Sci. Rep. 9, 14259.

Hackney, C.R., Darby, S.E., Parsons, D.R., Leyland, J., Best, J.L., Aalto, R., Nicholas, A.P., Houseago, R.C., 2020. River bank instability from unsustainable sand mining in the lower Mekong River. Nat. Sustain. 3, 217–225.

Hackney, C.R., Vasilopoulos, G., Heng, S., Darbari, V., Walker, S., Parsons, D.R., 2021. Sand mining far outpaces natural supply in a large alluvial river. Earth Surf. Dyn. 9, 1323–1334.

He, K., Zhang, X., Ren, S., Sun, J., 2016. Deep residual learning for image recognition. 2016 IEEE Conference on Computer Vision and Pattern Recognition (CVPR), 27-30 June 2016, pp. 770–778.

Hung, Le Manh, 2013. Research on Effects of Sand Mining Activities to Changes in Tien And Hau Rivers And Proposed Solutions for Sand Mining Management And Planning. Ministry of Science and Technology and Ministry of Agriculture and Rural Development, Ho Chi Minh city, Vietnam.

Iervolino, P., Guida, R., 2017. A novel ship detector based on the generalized-likelihood ratio test for SAR imagery. IEEE J. Sel. Top. Appl. Earth Obs. Remote Sens. 10, 3616–3630.

Jin, K., Chen, Y., Xu, B., Yin, J., Wang, X., Yang, J., 2020. A patch-to-pixel convolutional neural network for small ship detection with PolSAR images. IEEE Trans. Geosci. Remote Sens. 58, 6623–6638.

Meijer, L.J.J., van Emmerik, T., van der Ent, R., Schmidt, C., Lebreton, L., 2021. More than 1000 rivers account for 80% of global riverine plastic emissions into the ocean. Sci. Adv. 7, eaaz5803.

Monna, F., Rolland, T., Denaire, A., Navarro, N., Granjon, L., Barbé, R., Chateau-Smith, C., 2021. Deep learning to detect built cultural heritage from satellite imagery. - spatial distribution and size of vernacular houses in Sumba, Indonesia. J. Cult. Herit. 52, 171–183.

MONRE, 2015. Proposed Solution for Exploiting Sand to Serve the Key Projects. Ministry of Environment and Natural Resources, Ha Noi, Vietnam.

Nguyen, N.-D., Do, T., Ngo, T.D., Le, D.-D., 2020. An evaluation of deep learning methods for small object detection. J. Electric. Comput. Eng. 2020, 3189691.

Nie, X., Duan, M., Ding, H., Hu, B., Wong, E.K., 2020. Attention mask R-CNN for ship detection and segmentation from remote sensing images. IEEE Access 8, 9325–9334.

Osborne, M., 2000. The strategic significance of the Mekong. Contemp. Southeast Asia 22, 429–444.

Planet Team, 2017. Planet application program interface: in space for life on Earth. San Francisco, CA https://api.planet.com.

Ren, S., He, K., Girshick, R., Sun, J., 2015. Faster R-CNN: towards real-time object detection with region proposal networks. Proceedings of the 28th International Conference on Neural Information Processing Systems. Vol. 1. MIT Press, Montreal, Canada.

Sanderson, E.W., Jaiteh, M., Levy, M.A., Redford, K.H., Wannebo, A.V., Woolmer, G., 2002. The Human Footprint and the Last of the Wild: the human footprint is a global map of human influence on the land surface, which suggests that human beings are stewards of nature, whether we like it or not. Bioscience 52, 891–904.

Slabbekoorn, H., Bouton, N., van Opzeeland, I., Coers, A., ten Cate, C., Popper, A.N., 2010. A noisy spring: the impact of globally rising underwater sound levels on fish. Trends Ecol. Evol. 25, 419–427.

Tessler, Z.D., Vörösmarty, C.J., Grossberg, M., Gladkova, I., Aizenman, H., Syvitski, J.P.M., Foufoula-Georgiou, E., 2015. Profiling risk and sustainability in coastal deltas of the world. Science 349, 638–643.

Tickner, D., Opperman, J.J., Abell, R., Acreman, M., Arthington, A.H., Bunn, S.E., Cooke, S.J., Dalton, J., Darwall, W., Edwards, G., Harrison, I., Hughes, K., Jones, T., Leclère, D., Lynch, A.J., Leonard, P., McClain, M.E., Muruven, D., Olden, J.D., Ormerod, S.J., Robinson, J., Tharme, R.E., Thieme, M., Tockner, K., Wright, M., Young, L., 2020. Bending the curve of global freshwater biodiversity loss: an emergency recovery plan. Bioscience 70, 330–342.

Tzutalin, D., 2015. LabelImg. GitHub Repository. 6.

Vasilopoulos, G., Quan, Q.L., Parsons, D.R., Darby, S.E., Tri, V.P.D., Hung, N.N., Haigh, I.D., Voepel, H.E., Nicholas, A.P., Aalto, R., 2021. Establishing sustainable sediment budgets is critical for climate-resilient mega-deltas. Environ. Res. Lett. 16, 064089.

Venter, O., Sanderson, E.W., Magrach, A., Allan, J.R., Beher, J., Jones, K.R., Possingham, H.P., Laurance, W.F., Wood, P., Fekete, B.M., Levy, M.A., Watson, J.E.M., 2016. Sixteen years of change in the global terrestrial human footprint and implications for biodiversity conservation. Nat. Commun. 7, 12558.

Vnexpress, 2020a. Illegal clay mining in the Hau River [Online].Available: https://vnexpress.net/khai-thac-trai-phep-dat-set-duoi-song-hau-4076480.html Accessed 08/07/2022.

Vnexpress, 2020b. Illegal sand miners make hay as COVID-19 keeps people at home [Online]. Available: https://e.vnexpress.net/news/news/illegal-sand-miners-make-hay-as-covid-19-keeps-people-at-home-4086981.html Accessed 08/07/2022.

Wang, Z.-T., Akamatsu, T., Duan, P.-X., Zhou, L., Yuan, J., Li, J., Lei, P.-Y., Chen, Y.-W., Yang, Y.-N., Wang, K.-X., Wang, D., 2020. Underwater noise pollution in China's Yangtze River critically endangers Yangtze finless porpoises (Neophocaena asiaeorientalis asiaeorientalis). Environ. Pollut. 262, 114310.

Wilkinson, J.L., Boxall, A.B.A., Kolpin, D.W., Leung, K.M.Y., Lai, R.W.S., Galbán-Malagón, C., Adell, A.D., Mondon, J., Metian, M., Marchant, R.A., Bouzas-Monroy, A., Cuni-Sanchez, A., Coors, A., Carriquiriborde, P., Rojo, M., Gordon, C., Cara, M., Moermond, M., Luarte, T., Petrosyan, V., Perikhanyan, Y., Mahon, C.S., McGurk, C.J., Hofmann, T., Kormoker, T., Iniguez, V., Guzman-Otazo, J., Tavares, J.L., Gildasio de Figueiredo, F., Razzolini, M.T.P., Dougnon, V., Gbaguidi, G., Traoré, O., Blais, J.M., Kimpe, L.E., Wong, M., Wong, D., Ntchantcho, R., Pizarro, J., Ying, G.-G., Chen, C.-E., Páez, M., Martínez-Lara, J., Otamonga, J.-P., Poté, J., Ifo, S.A., Wilson, P., Echeverría-Sáenz, S., Udikovic-Kolic, N., Milakovic, M., Fatta-Kassinos, D., Ioannou-Ttofa, L., Belušová, V., Vymazal, J., Cárdenas-Bustamante, M., Kassa, B.A., Garric, J., Chaumot, A., Gibba, P., Kunchulia, I., Seidensticker, S., Lyberatos, G., Halldórsson, H.P., Melling, M., Shashidhar, T., Lamba, M., Nastiti, A., Supriatin, A., Pourang, N., Abedini, A., Abdullah, O., Gharbia, S.S., Pilla, F., Chefetz, B., Topaz, T., Yao, K.M., Aubakirova, B., Beisenova, R., Olaka, L., Mulu, J.K., Chatanga, P., Ntuli, V., Blama, N.T., Sherif, S., Aris, A.Z., Looi, L.J., Niang, M., Traore, S.T., Oldenkamp, R., Ogunbanwo, O., Ashfaq, M., Iqbal, M., Abdeen, Z., O'Dea, A., Morales-Saldaña, J.M., Custodio, M., de la Cruz, H., Navarrete, I., Carvalho, F., Gogra, A.B., et al., 2022. Pharmaceutical pollution of the world's rivers. Proc. Natl. Acad. Sci. 119, e2113947119.

Yang, H., Cao, Z., Cui, Z., Pi, Y., 2019. Saliency detection of targets in polarimetric SAR images based on globally weighted perturbation filters. ISPRS J. Photogramm. Remote Sens. 147, 65–79.

Zajicek, P., Wolter, C., 2019. The effects of recreational and commercial navigation on fish assemblages in large rivers. Sci. Total Environ. 646, 1304–1314.

Zhang, S., Wu, R., Xu, K., Wang, J., Sun, W., 2019. R-CNN-based ship detection from high resolution remote sensing imagery. Remote Sens. 11, 631.

Zhang, T., Zhang, X., Shi, J., Wei, S., 2020. HyperLi-Net: a hyper-light deep learning network for high-accurate and high-speed ship detection from synthetic aperture radar imagery. ISPRS J. Photogramm. Remote Sens. 167, 123–153.

Zhang, T., Zhang, X., Liu, C., Shi, J., Wei, S., Ahmad, I., Zhan, X., Zhou, Y., Pan, D., Li, J., Su, H., 2021. Balance learning for ship detection from synthetic aperture radar remote sensing imagery. ISPRS J. Photogramm. Remote Sens. 182, 190–207.

Zhou, Y., Liu, L., Shao, L., Mellor, M., 2018. Fast automatic vehicle annotation for urban traffic surveillance. IEEE Trans. Intell. Transp. Syst. 19, 1973–1984.